Proceedings of Global Power and Propulsion Society
ISSN-Nr: 2504-4400
Beijing Conference 2019
16th – 18th September, 2019
www.gpps.global

GPPS-BJ-2019-0019

Enhanced Heat Transfer of Jet Impingement Nozzle with Piezoelectric Fan

Lin Yuan
Shanghai Jiao Tong University
yuanlin@sjtu.edu.cn
Shanghai, China

*** Wenwu Zhou**
Shanghai Jiao Tong University
zhouww@sjtu.edu.cn
Shanghai, China

Yingzheng Liu
Shanghai Jiao Tong University
yzliu@sjtu.edu.cn
Shanghai, China

ABSTRACT

Heat transfer performance of a newly designed jet impingement nozzle was studied in this research. An oscillating blade-fan is mounted at the nozzle exit. The heat transfer results of the impinging surface were reduced through the temperature-sensitive paint (TSP) technology. Different nozzle-to-surface spacings and flow rate (Re = 5000, 10000, 18000) were conducted in the experiments. The results show that smaller nozzle-to-surface spacings and larger flow rate yield better heat transfer rate compared with traditional long pipe nozzle, with the maximum 20% enhancement near the stagnation point. The flow field experiments were also conducted with the Planer-PIV technique trying to explain the inherent mechanism.

INTRODUCTION

Jet impingement flow produces higher heat transfer rate compared with other methods of heat exchange. It is widely applied in the industry such as the internal cooling inside the turbine blades, air foil de-icing, electron component cooling (Zuckerman & Lior., 2005).

The heat transfer rate of typical jet impingements is related to parameters such as flow rate, nozzle-to-surface spacings, nozzle geometry, etc. The Nusselt number distributions over the impinging surface have been studied and reviewed by many authors (Jambunathan et al., 1992) (Zuckerman & Lior., 2005). According to those data, the Nusselt number always decreases in the radial direction, although small peaks may occur at narrow nozzle-to-surface spacings (Gardon & Akfirat 1965). For a long round pipe nozzle, the Nusselt number decreases 4 to 5 magnitude from the stagnation point to the normalized radial location r/D = 9.0 (Zuckerman et al., 2005). But for industrial applications, both high and uniform distribution of heat transfer rate is a more promising option, which means fewer nozzles of arrays and less energy consumption.

To achieve this goal, the sweeping jet issued from a Fluidic Oscillator (Raghu, 2013) is a typical device for a wider range of heat transfer maps. (Park et al., 2018) experimented the heat transfer maps of the sweeping jet impingement and its flow structure. The authors concluded that the unsteadiness near the stagnation region causes high heat exchange. (Zhou et al., 2019) studied the heat transfer of the sweeping jet at narrow spacing and found that the sweeping jet covers lager area of high heat transfer rate. (Wen et al., 2018) looked into the flow structure of the sweeping and impinging jet with PIV techniques.

For our present study, the piezoelectric technique was used to design the new nozzle. The basic structure is illustrated in Figure 1(a). The Piezoelectric Fan (PE fan) consists of a long round pipe nozzle and a thin metallic blade. The blade is one-side coated with a layer of lead zirconate titanate (PZT) material (Alastair Hales & Xi Jiang, 2018). The PZT coating deforms when exposed to voltage differences, which will bend the blade. Thus, when AC voltage is applied between the PZT coating and the metallic blade, the PE fan starts to oscillate like a cantilever (Alastair Hales & Xi Jiang, 2018). The idea of the design is to widen the jet area with the oscillating PE blade, which would in turn cover more area of the impinging surface, such the work as (Zhou et al., 2019). Also, the power consumption of the device is very small ($\leq 10\ mW$) as the PE fan blade is analogous to capacitance (Alastair Hales & Xi Jiang, 2018).

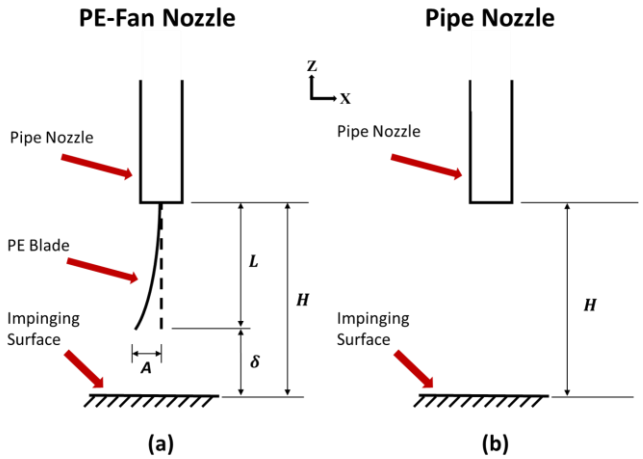

Figure 1 PE fan nozzle configuration

For published PE fan studies, most authors were focusing on oscillating in the natural convective environment, i.e. without the jet nozzle compared to our present study. More detail could be referred to in the reviewed papers by (Alastair Hales & Xi Jiang, 2018) and (Maaspuro, 2016). Here we focus more on the PE fan studies in the channel flow. (Florio & Harnoy, 2007) investigated a PE fan stand on a side-wall of a wind tunnel. The blade is parallel to flow stream and oscillates vertically. Their results showed that when the frequency and amplitude increases, the heat transfer rate of the surface under the blade (the down-side of the wind tunnel) enhances. Meanwhile, the heat transfer rate experienced a 52% increases when the PE fan was moved 1.5 X/D upstream of the original heat transfer measurement area. (Li et al., 2017) decreased the distance between the blade and the surface and discovered a proportional correlation between the distance and the heat transfer rate. (Jeng & Liu, 2015) also studied the flow field and heat transfer characteristic of PE fan in the channel flow. From data published by those authors, it could be concluded that the heat transfer increases due to PE fan are obvious only when the speed of the main flow is small. In other words, when the main flow is strong, the PE fan will not be an effective method for the enhancement of heat transfer. This also explains the reason that most studies concentrated on low Reynolds number applications.

EXPERIMENTAL SETUP

Apart from the PE fan nozzle mentioned in Figure 1 (a), a long round pipe nozzle without the PE blade as shown in Figure 1 (b) was used as the baseline. The inner diameter of both nozzle (D) is 15 mm. The PE fan blade, with the length L = 66 mm, width W = 15 mm and thickness of 0.2 mm, oscillates like a cantilever in x direction and has a tip amplitude of 8 mm when the input AC power frequency coupes with the natural frequency of the PE fan Nozzle (38.5 Hz). The AC input is equipped with a signal generator and a power amplifier. The effective voltage value applied to the PE fan is around 80 Ampere.

The flow rate is normalized to the Reynolds number, which includes three levels (Re = 5000, 10000, 18000). Note that the Reynolds number in this study is defined by the nozzle inner diameter and the nozzle jet exit speed. Three different nozzle-to-surface spacing were also investigated, H/D = 4.5, 5.5, 6.5. Note that for the PE fan nozzle, the H refers to the distance between the surface and the blade root, which means the actual gap between the surface and the blade tip δ/D is 0.1, 1.1, 2.1 corresponding to H/D = 4.5, 5.5, 6.5 respectively.

Heat transfer test rig

The facility used to measure the heat transfer rate is illustrated in Figure 2 (a). The air jet is supplied by a blower at room temperature and controlled by a valve and flow meter. The nozzle is installed on a traverse system which could move in the z-direction.

The impinging surface was shown in Figure 2(b). It consists of a thin stainless steel sheet and a layer of TSP coating underneath. Two beams were used to support and tension the stainless steel sheet. The tension of the stainless steel sheet could also be adjusted by moving the beams in the y-direction. The DC power is applied to two sides of the copper buses to generate Joule heat flux across the whole stainless steel sheet. The typical value of the DC power input is 50 Ampere and 1.5 Volt. Due to the thickness of the stainless steel sheet (δ_{foil} =30 μm) and it's thermal conductivity, the two-layer surface is considered isothermal in the direction of thickness (Raiola et al., 2017) (Astarita & Carlomagno 2012).

The TSP coating is utilized to measure the temperature field over the stainless steel sheet. When the LED light with the wavelength around 385 nm is projected to the TSP coating painted on the downside of the steel sheet (as showed in Figure 2), the TSP will emits a light with longer fixed wavelength. Meanwhile, the luminous intensity of the TSP is inversely proportional to the local temperature. A CCD camera with the resolution 1600×1200 captures the luminous intensity of the stainless steel sheet, which will be transferred to temperate field by a calibration process (Zhou et al., 2019). A band-pass filter (600±25 nm) is mounted to the camera in order to get rid of the light other than the TSP emitting wavelength.

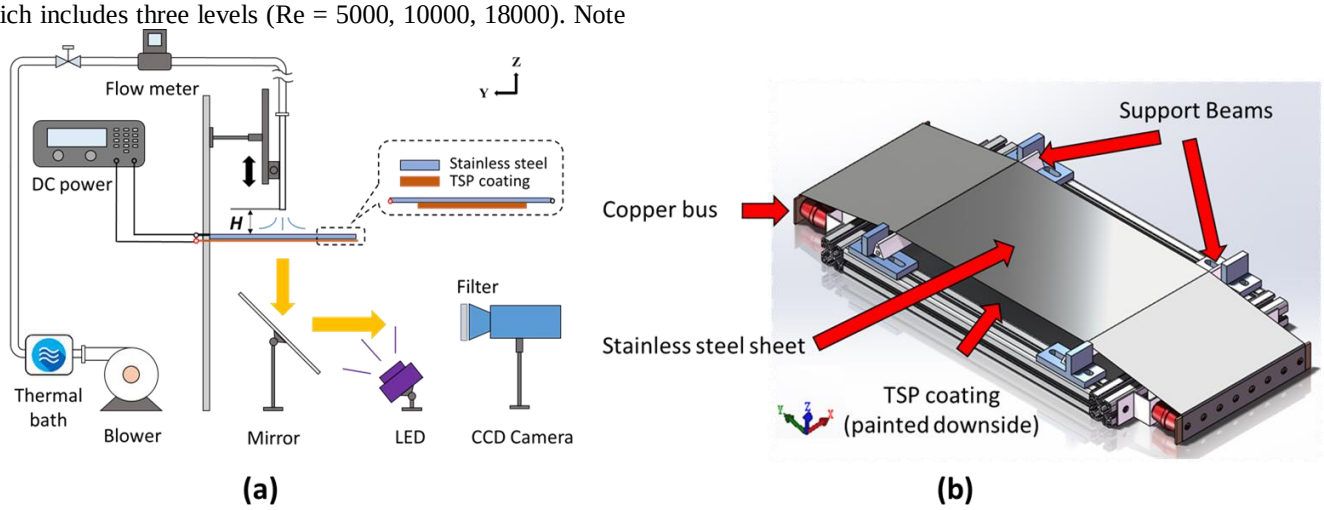

Figure 2 Heat transfer test setup: (a) overall setup and (b) detail of impinging surface model

The Nusselt number were calculated through the equation:

$$Nu = D \cdot \frac{q_j + q_{tan} - q_{rad} - q_{nc}}{k_j \cdot (T_w - T_j)}, \quad (1)$$

where q_j represents the total Joule heat flux applied by the DC power to the stainless steel, whose values were controlled between $1000 \sim 2500\ W/m^2$ in the experiments. k_j is the thermal conductivity of the jet fluid.

q_{tan} represents the tangential heat transfer within the stainless steel sheet. It evaluates the heat transfer within the thin foil (i.e., in x and y directions). The calculation of this parameter can be referred to the works by (Carlomagno & Cardone 2010), (Astarita & Carlomagno 2012) and (Crispo et al., 2018) with the following equations:

$$q_{tan} = -k_{foil} \cdot \delta_{foil} \nabla^2 T_w, \quad (2)$$

where k_{foil} refers to the thermal conductivity of the stainless steel sheet and $\nabla^2 T_w$ indicates a second-order differential over the temperature captured at the impinging surface. In present study, the actual contribution of this value is less than 0.8 % of total q_j.

q_{rad} is the radiation heat loss due to the heating of the impinging surface and was estimated through equation:

$$q_{rad} = \sigma\varepsilon(T_w^4 - T_{amb}^4). \quad (3)$$

where σ is the Stefan-Boltzmann's constant, and ε refers to the surface emissivity. The contribution of q_{rad} is less than 11% of total q_j.

q_{nc} is the natural convective heat loss from the downside of the impinging surface. In practical, this value was estimated by the correlation function literature by (Hassan & Mohamed, 1970) and (Kays et al., 2012):

$$Nu_{nc} = 0.27(Gr \cdot Pr)^{1/4}, \quad (4)$$

where Gr and Pr are the Grashof number and Prandtl number of air respectively. Note that the Nusselt number Nu_{nc} were calculated within the subject of the natural convective heat loss. The typical contribution of q_{nc} is less than 7.5 % in present study.

T_w represents the temperature maps captured by the TSP system. The temperature of the jet (T_j) was measured by a T-type thermocouple at the exit of the nozzle. T_{amb} was measured as the ambient temperature with the same type of thermocouple. k_j refers to the thermal conductivity of the air jet.

The typical values from Equation (1) are listed in Table 1. The uncertainty of the TSP was accessed after the calibration process according to the method from (Johnson & Hu, 2016), which was considered as a contributor to the uncertainty of measured T_w. The maximum uncertainty always appears at the region of the stagnation point. The major contribution of the uncertainty to the final Nusselt number is $(T_w - T_j)$. Thus, the maximum uncertainty always appears at the region near the stagnation point. For most cases, the uncertainty of Nusselt number is around 9%, and for cases with high Reynolds number, the uncertainties of Nusselt number are less than 13%. The method used to evaluate the uncertainties is suggested by (Moffat, 1988).

Table 1 Measurement Uncertainties

	Typical value	Uncertainty
TSP	---	0.6 K
T_j	298 K	0.5 K
T_w	308 K	0.7 K
U	2 V	1%
I	50 A	1%
T_{amb}	298 K	0.5 K
$T_w - T_j$	10 K	0.85 K

A validation process was conducted comparing the data from (Lytle & Webb, 1994) and (Katti & Prabhu, 2008) to assure the reliability of the heat transfer result (as showed in Figure 3).

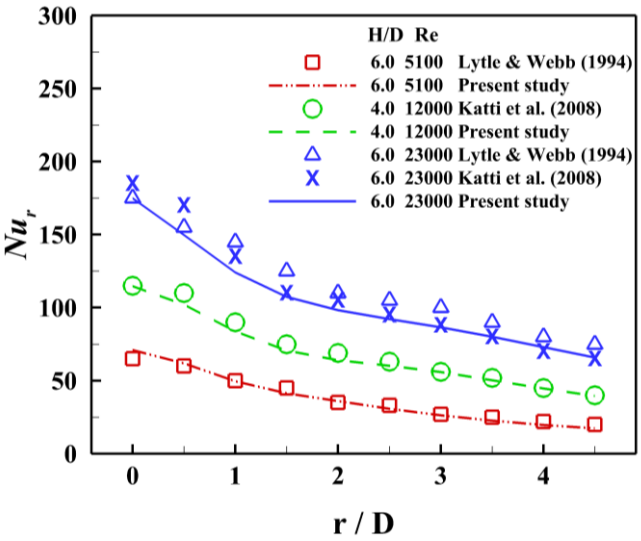

Figure 3 Heat transfer validation results

Planar-PIV test rig

The flow field was measured by the PIV facility showed in Figure 4. The impinging surface in Figure 2 was changed to a transparent Plexiglas which along the laser to pass through. The laser sheet was produced in the xOz plane by a class IV pulse laser product with the sampling frequency of 1.0 Hz. The max power output is 800 mJ during every 4 ns pulsation. During every sampling, a pair of images (2 images) was acquired in a precise time interval and then reduced to velocity field data. The jet was seeded with ~1 μm oil droplets. A high-resolution digital camera (4872×3248 pixels) was used for the acquisition of PIV images. In the experiments, sets of 800 images were successively recorded. The standard PIV cross-correlation algorithm was used to resolve the flow fields. A interrogation window of 32×32 pixels and 50% overlap were applied for the velocity calculation. The error between two images pair is smaller than 0.1 pixels, which means the uncertainty of x- and z-direction velocity are estimated to be less than 2%.

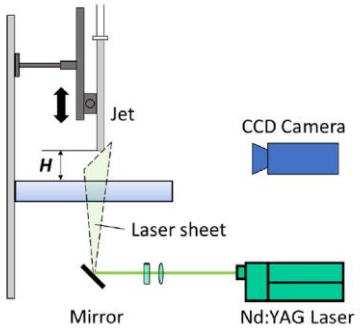

Figure 4 Schematic diagram of Planar-PIV setup

RESULTS AND DISCUSSION

Heat transfer results

Figure 5 shows the Nusselt number contour at H/D = 4.5. Note that the legend levels are different for three Reynolds number cases. Comparing the left and the right row, higher heat transfer rate of PE-Fan were observed for all three Reynolds number at the nozzle-to-surface spacing H/D = 4.5 (δ/D = 0.1).

From the right row of PE Fan Re = 5000 case in Figure 5, the high heat transfer region locates mostly in the center, while for higher Reynolds number, three distinct high heat transfer region occurs along the vibrating direction. This phenomenon is weakened for higher nozzle-to-surface spacing, which was concluded from the peak shape of the Nusselt number from Figure 6(a).

Figure 6 presents the Nusselt Number along the vibrating direction at y = 0. In Figure 6(a), when the nozzle-to-surface spacing is small (i.e. H/D = 4.5 (δ/D = 0.1)), higher Reynolds number leads to better heat transfer enhancement for the PE fan than that of the pipe nozzle. As the Reynolds number decreases, the curves of PE fan move closer to the data of pipe nozzle. For the case of H/D = 4.5 and Re = 5000, the curve almost coincides with its baseline data, but of different shape in the middle.

For H/D = 5.5 (δ/D = 0.1) in Figure 6 (b), the heat transfer rate is no longer promising as that of H/D = 4.5. High Reynolds number configuration (Re = 18000) showed approximate 20% enhancement near the stagnation region.

With the decrease of Reynolds number, the enhancement drops as well, even below the pipe nozzle. This trend can also be concluded in Figure 6(c). For cases where "worse" heat transfer occurs, the Nusselt number shows a "flat" curve in the stagnation region (red solid line in Figure 6(b) and Figure 6(c)).

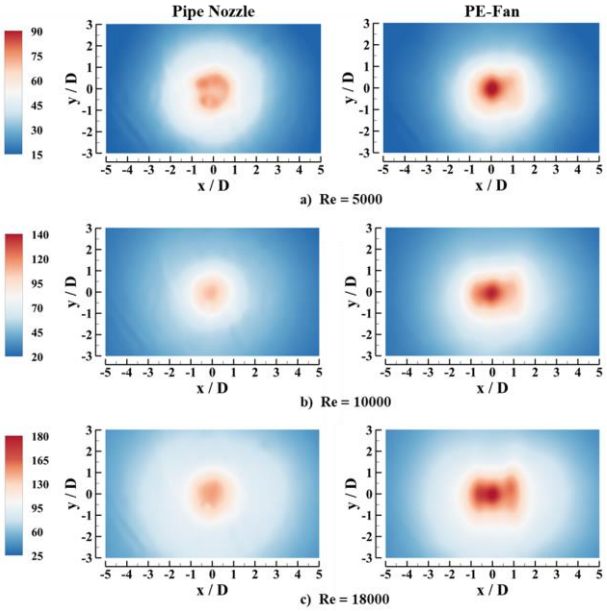

Figure 5 Nusselt No. distribution at H/D=4.5

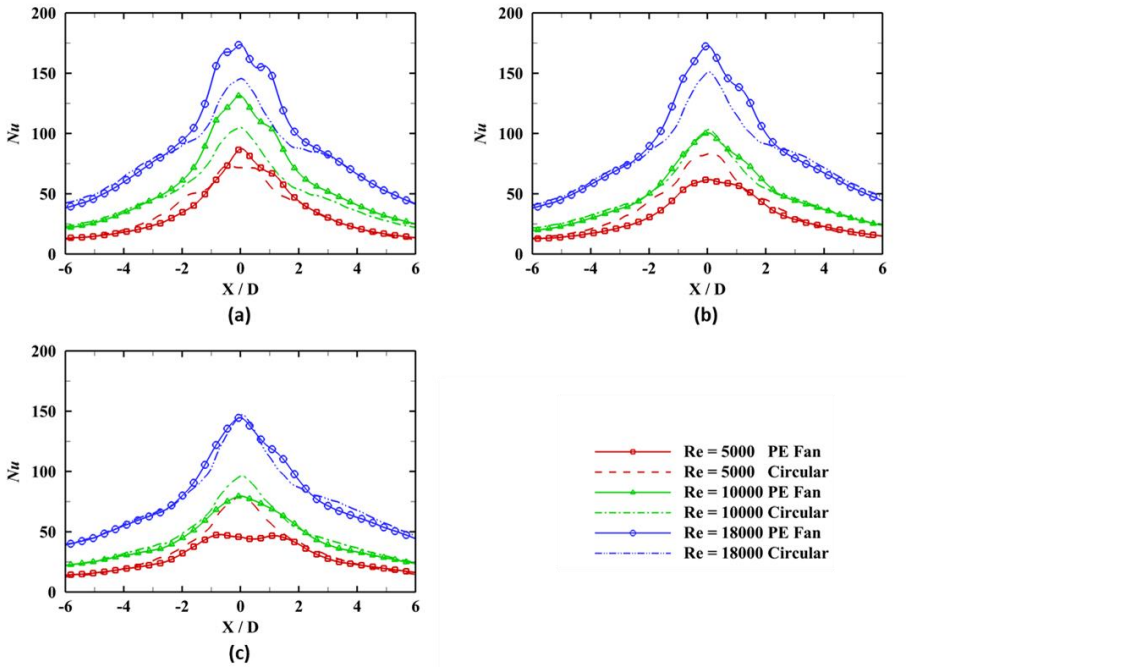

Figure 6 Nusselt number of impinging surface at y=0 with difference H/D: (a) H/D=4.5, (b) H/D=5.5, (c) H/D=6.5

Figure 6 only showed the line data at the location where y=0. In order to analysis the heat transfer rate of the whole surface, the azimuthally averaged radial Nusselt number is defined and calculated by Equation (5). The results are presented in Figure 6 in term of relative value in contrast with pipe nozzle.

$$Nu_r = \frac{1}{2\pi}\int_0^{2\pi} Nu(r,\theta)d\theta \qquad (5)$$

$$\xi = \frac{Nu_{r,PE}}{Nu_{r,pipe}} \qquad (6)$$

The point where r = 0 indicates the stagnation point of the pipe nozzle jet. The enhancement ratio, ξ, is introduced to represent the heat transfer performance, which is calculated through Equation (6). Value greater than one indicates the PE fan has a better performance than the corresponding traditional pipe nozzle. Value smaller than one, accordingly, expresses the worse heat transfer rate.

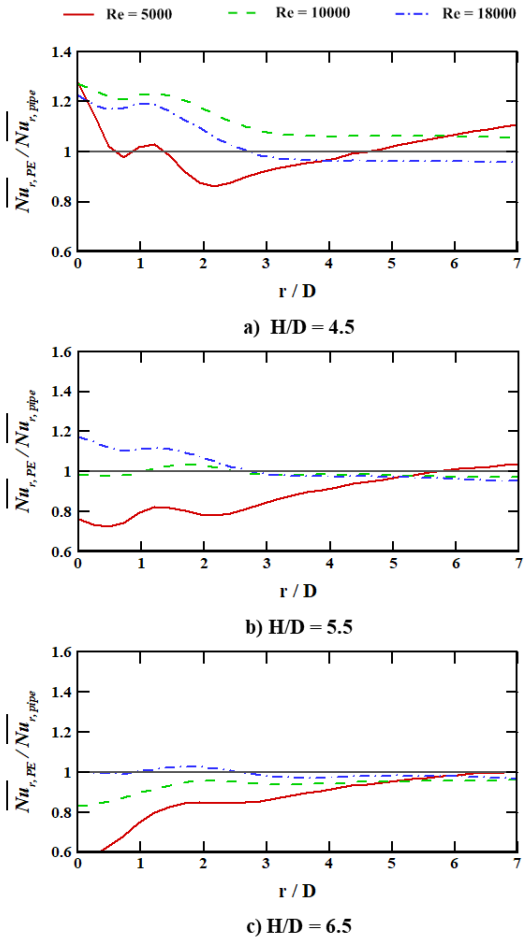

Figure 7 Hear transfer enhancement ratio

Figure 7 plots this enhancement ratio of some cases. According to Figure 7, it could be concluded that closer spacing shows better trends of enhanced heat transfer. For the case H/D = 4.5 (i.e. δ/D = 0.1) and Re=5000, stagnation region and radial location $r/D > 5$ show good enhancement. For higher Reynolds number, the enhancement region stays within $r/D < 2.5$ and exceed 10% where $r/D < 1.5$. the maximum enhancement reaches 20% compared with pipe nozzle. As H/D increases, enhancement drops. Lower Reynolds number shows smaller enhancement ratio. Only the Re = 18000 case has an enhancement ratio lager than one, which lies within $r/D < 2.5$.

The different heat transfer rate between the PE fan nozzle and pipe nozzle concentrates mostly near the stagnation point. The Nusselt number with larger r/D show neither better nor worse enhancement. Comparing the surface Nusselt number of PE fan nozzle and pipe nozzle with various Re and H/D, the heat transfer enhancement could be concluded as either effective or worse. And the difference concentrates mostly near the stagnation point. The Nusselt number of two configurations at larger r/D overlaps. However, the underlying cause of such heat transfer map may differ. To better understand this mechanism, Planar-PIV results are presented and analyzed.

Flow analysis

The velocity profile was acquired and established at the xOz plane for all the cases. The purpose of this part of the experiment is to look in the flow detail of such PE-fan configuration and try to explain the heat transfer though the flow field result.

The movement of our PE fan nozzle is, to some extent, similar to that of a typical PE-fan, except than jet flow is introduced. For the typical PE-fan without the jet, as the blade vibrates, the vortex caused by pressure difference forms at the tip location and then shades off, which was concluded by (Choi et al., 2012) to four steps: initiation, development, separation and propagation. However, the flow speed induced by such is usually small. When the jet flow is applied, the vortex generated by the above-mentioned mechanism will no longer maintain its integrity. Strong turbulence was observed for Re = 5000 and Re = 18000 as shown in Figure 8. Five averaged phase were selected with the phase 0.2π, 0.4π, 0.6π, 0.8π and 1.0π in top-down order.

Obviously, the vortex structure is distinctive from that in Figure 9 (Choi et al., 2012). The documented counter-rotating vortex pair propagated from the blade tip was suppressed and broken into small and line-distributed eddies due to the impinging jet vertex issued from the nozzle (Figure 8). The pair of vortex core showed in figure 9 disappears and only the tip shear layer region which connects the blade tip and the core remains.

When the jet speed is relatively small (Figure 8(a)), the laminar boundary can still be observed at either side of the blade root. As the blade moves outwards, the jet, which would flow vertically, was sucked to the blade tip due to lower pressure and interact with the tip tail vertex. When the blade reaches its maximum position, both tip vortex and nozzle jet vertex are thrown out onto the impinging surface like an “S” shape. When the PE fan is exposed to high Reynolds number, the suction from the blade is less obvious and the jet flow is more turbulent-dominated as depicted in figure 8(b). As the blade is at its maximum position, the jet vortex cores no longer moves inward to the stagnation point with the “S” shape but directly stretch out.

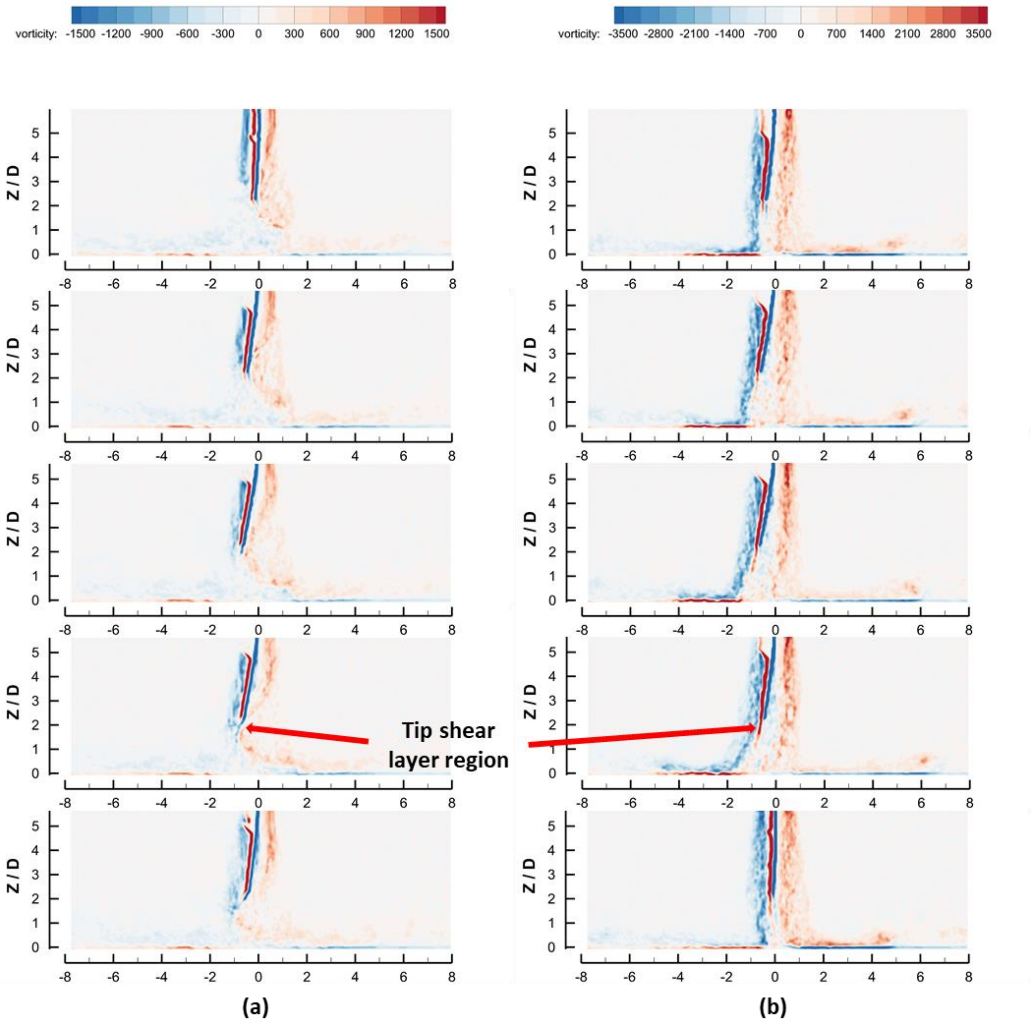

Figure 8 Instantaneous vorticity distribution of (a) Re = 5000, (b) Re = 18000 at xOz plane

Although it is hard for such large scale vortex to exist in the PE fan nozzle configuration, heat transfer enhancement does happen when the blade is very close to the impinging surface as shown in Figure 6(a).

As discussed from Figure 8, high shear layer exits on both sides of the blade. The shear layer extends out from the blade tip to form a tail-like region (i.e. the tip shear layer region). When the blade is positioned very close to the impinging surface (δ/D=0.1), this tip shear layer region interacts with the wall.

Figure 10 shows the x-direction velocity and RMS velocity distribution of such close spacing (Re=18000, H/D=4.5 i.e. δ =1.5mm). This may give a concept of such interaction from another indirect perspective. The data was reduced from the time-averaged xOz-plane PIV results. Pipe nozzle flow field is also acquired as the baseline. When the location is close to the stagnation point, the RMS velocity is always larger than pipe nozzle. This is due to the vibration of the blade. As the distribution where X/D=0.5 shows, the vibrating leads to higher RMS velocity at the range of Z/D=0 to Z/D=1.0. As the air flows outwards, the differences of RMS velocity become smaller and become closer to the wall (Figure (b)). At X/D = 3.0, both velocity and RMS velocity distribution of two kinds of nozzle almost overlap. This is consistent with the conclusion from the heat transfer results.

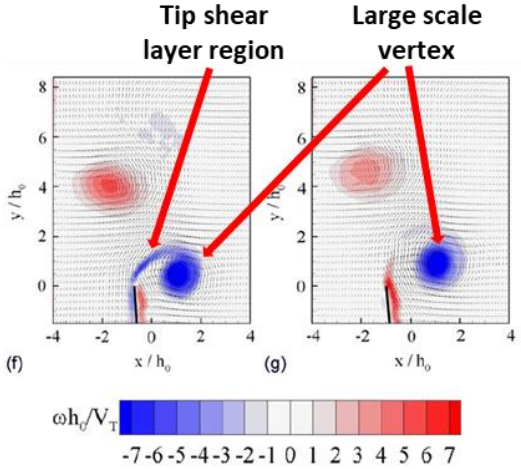

Figure 9 Vorticity distribution reproduced from (Choi et al., 2012)

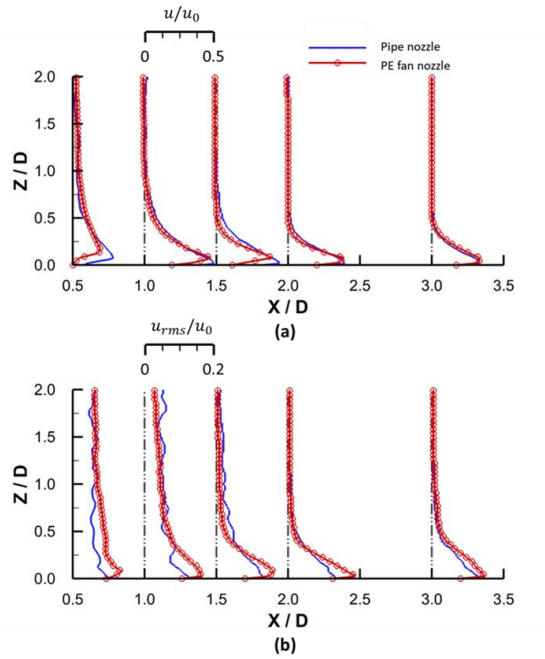

Figure 10 x-direction (a) velocity and (b) RMS velocity distribution of Re=18000 H/D=4.5

As the blade vibrating frequency and amplitude is fixed, the tip velocity is also a constant. Nevertheless, a higher Reynolds number (Re=18000, Re=10000) yield better enhancement. Which implies that the jet from the nozzle also attributes to the blade tip interaction with the wall.

As the H/D increases, the potential for the tip shear layer to reach the heated surface decreases. The loss of the velocity due to vibrating no longer compensates the entrainment of the cold air, which appears as "worse" enhancement as H/D = 4.5 Re = 5000 in Figure 6(c).

Either the tip shear layer or the RMS analysis only gives a general view of how the blade enhances heat transfer. We believe than the core of such physics lies in the gap between the blade tip and the impinging surface. However this gap is very small (δ =1.5mm) and the conclusion was drown only base on some lager flow characteristics. Further study is needed focusing on this gap region if more details are required.

CONCLUSIONS

In the present study, a new type of jet impingement nozzle with PE fan was designed. Heat transfer experiments and PIV measurement were carried out to test its performance. Results show that when the blade tip is close to the impinging surface, the Nusselt number will yields a 20% enhancement with near the stagnation region (Re =18000, H/D =4.5 i.e. δ/D =0.1). Closer H/D and higher Reynolds number lead to higher enhancement ratio. A maximum enhancement of 20% was observed during the conducted experimental cases within the stagnation region.

High enhancement always happens near the stagnation region. As jet flow moves away from the center, the heat transfer difference between the PE fan and the pipe nozzle becomes minor.

The flow field was acquired at xOz plane. The presence of nozzle jet suppressed the formation of large scale vertices and leaving only the tip shear layer region swinging with the blade tip. The tip shear layer region interacts with the impinging surface when close enough, which causes the heat transfer enhancement in the stagnation region.

NOMENCLATURE

A	tip amplitude of the PE fan
D	nozzle diameter/PE fan width
H	distance between nozzle exit and impinging surface
I	input current of q_j
L	PE fan Length
Re	Reynolds number based on D and u_0
U	input voltage of q_j
W	PE fan width
k_j	thermal conductivity of air jet
k_{foil}	thermal conductivity of the stainless steel sheet
Nu	surface Nusselt number
Nu_r	azimuthally averaged Nusselt number
q_j	Joule heat input by DC power
q_{nc}	natural convection heat loss from the down-side of the impinging surface
q_{rad}	radiation heat loss from both side of the impinging surface
q_{tan}	tangential heat loss within the impinging surface
r	radial coordinate
T_{amb}	ambient air temperature
T_j	jet temperature
T_w	temperature of
u	x-direction velocity
u_0	nozzle exit mean velocity
u_{rms}	x-direction RMS velocity

Greek symbols

δ	gap between PE fan tip and impinging surface
δ_{foil}	thickness of the stainless steel sheet
ε	surface emissivity
θ	azimuthal angle
ξ	enhancement ratio
σ	Stefan-Boltzmann's constant

ACKNOWLEDGMENTS

The authors acknowledge the financial support from the National Natural Science Foundation of China (11725209, 51806138) and the Shanghai Sailing Program (18YF1411300).

References

Astarita T., Carlomagno G.M. (2012). Infrared Thermography for Thermo-Fluid-Dynamics, Springer Science & Business Media.

Carlomagno G.M., Cardone G. (2010). Infrared thermography for convective heat transfer measurements. Exp. Fluids 49 (6), 1187–1218. doi: 10.1007/s00348-010-0912-2

Choi M., Cierpka C., Kim Y.-H. (2012). Vortex formation by a vibrating cantilever. Journal of Fluids and Structures 31, 67–78. doi: 10.1016/j.jfluidstructs.2012.03.004

Crispo C. M., Greco C. S., Cardone G. (2018). Convective heat transfer in circular and chevron impinging synthetic jets. International Journal of Heat and Mass Transfer 126, 969-979. doi: 10.1016/j.ijheatmasstransfer.2018.06.062

Florio LA., Harnoy A. (2007). Use of a vibrating plate to enhance natural convection cooling of a discrete heat source in a vertical channel. Appl Therm Eng 27 (13), 2276–93. doi: 10.1016/j.applthermaleng.2007.01.023

Gardon R., Akfirat I.C.(1965). The role of turbulence in determining the heat transfer characteristics of impinging jets. Int. f. Heal Mass 8, 1261-J 172.

Hales A., Jiang X. (2018). A review of piezoelectric fans for low energy cooling of power electronics. Applied Energy 215, 321–337. doi: 10.1016/j.apenergy.2018.02.014

Hassan K.-E., Mohamed S.A. (1970). Natural convection from isothermal flat surfaces. Int. J. Heat Mass Transf. 13 (12), 1873–1886. doi: 10.1016/0017-9310(70)90090-6

Jambunathan K., Lai K., M. A. Moss M. A., Button B. L. (1992). A review of heat transfer data for single circular jet impingement. Int. J. Heat and Fluid Flow 13.

Jeng TM, Liu CH. (2015). Moving-orientation and position effects of the piezoelectric fan on thermal characteristics of the heat sink partially filled in a channel with axial flow. Int J Heat Mass Transfer 85, 950–64. doi: 10.1016/j.ijheatmasstransfer.2015.02.053

Johnson B, Hu H. (2016). Measurement Uncertainty Analysis in Determining Adiabatic Film Cooling Effectiveness by Using Pressure Sensitive Paint Technique. Journal of Turbomachinery 138(12), 121004. doi: 10.1115/1.4033506

Kays W.M., Crawford M.E., Weigand B. (2012). Convective Heat and Mass Transfer. Tata McGraw-Hill Education.

Katti V., Prabhu S.V. (2008). Experimental study and theoretical analysis of local heat transfer distribution between smooth flat surface and impinging air jet from a circular straight pipe nozzle. International Journal of Heat and Mass Transfer 51, 4480–4495. doi: 10.1016/j.ijheatmasstransfer.2007.12.024

Li X., Zhang J., Tan X. (2017). Convective heat transfer on a flat surface induced by a vertically-oriented piezoelectric fan in the presence of cross flow. Heat Mass Transfer 53 (9), 2745–68. doi: 10.1007/s00231-017-2019-2

Maaspuro M. (2016). Piezoelectric oscillating cantilever fan for thermal management of electronics and LEDs — A review. Microelectronics Reliability 63, 342–353. doi: 10.1016/j.microrel.2016.06.008

Moffat R.J. (1998). Describing the uncertainties in experimental results. Exp. Therm.Fluid Sci. 1 (1), 3–17.

Park T., Kara K., Kim D. (2018). Flow structure and heat transfer of a sweeping jet impinging on a flat wall. International Journal of Heat and Mass Transfer 124, 920-928. doi: 10.1016/j.ijheatmasstransfer.2018.04.016

Raghu S. (2013). Fluidic oscillators for flow control, Exp. Fluids 54, 1455. doi: 10.1007/s00348-012-1455-5

Raiola M., Greco C. S., Contino M., Discetti S., Ianiro A. (2017). Towards enabling time-resolved measurements of turbulent convective heat transfer maps with IR thermography and a heated thin foil. International Journal of Heat and Mass Transfer 108, 199–209. doi: 10.1016/j.ijheatmasstransfer.2016.12.002

Wen X., Liu Y., Tang H. (2018). Unsteady behavior of a sweeping impinging jet: Time-resolved particle image velocimetry measurements. Experimental Thermal and Fluid Science 96, 111-127. doi: 10.1016/j.expthermflusci.2018.02.033

Zhou W., Yuan L., Liu Y., Peng D., Wen X. (2019). Heat transfer of a sweeping jet impinging at narrow spacings. Experimental Thermal and Fluid Science 103, 89-98. doi: 10.1016/j.expthermflusci.2019.01.007

Zuckerman N., Lior N. (2005). Jet impingement heat transfer: physics, correlations and numerical modelling. Advances in heat transfer 39, 565-631. doi:10.1016/S0065-2717(06)39006-5

Zhou W., Yuan L., Liu Y., Peng D., Wen X. (2019). Heat transfer of a sweeping jet impinging at narrow spacings. Experimental Thermal and Fluid Science 103, 89-98. doi: 10.1016/j.expthermflusci.2019.01.007

Zuckerman N., Lior N. (2005). Jet impingement heat transfer: physics, correlations and numerical modelling. Advances in heat transfer 39, 565-631. doi:10.1016/S0065-2717(06)39006-5